Functional integrity of the contractile actin cortex is safeguarded by multiple Diaphanous-related formins

Christof Litschko[a,1], Stefan Brühmann[a,1], Agnes Csiszár[b], Till Stephan[a], Vanessa Dimchev[c,d], Julia Damiano-Guercio[a], Alexander Junemann[a], Sarah Körber[a], Moritz Winterhoff[a], Benjamin Nordholz[a,2], Nagendran Ramalingam[e], Michelle Peckham[f], Klemens Rottner[c,d], Rudolf Merkel[b], and Jan Faix[a,3]

[a]Institute for Biophysical Chemistry, Hannover Medical School, 30625 Hannover, Germany; [b]Institute of Complex Systems, ICS-7: Biomechanics, Forschungszentrum Jülich GmbH, 52425 Jülich, Germany; [c]Division of Molecular Cell Biology, Zoological Institute, Technische Universität Braunschweig, 38106 Braunschweig, Germany; [d]Molecular Cell Biology Group, Helmholtz Centre for Infection Research, 38124 Braunschweig, Germany; [e]Ann Romney Center for Neurologic Diseases, Brigham and Women's Hospital, Harvard Medical School, Boston, MA 02115; and [f]Astbury Centre for Structural Molecular Biology, University of Leeds, Leeds LS2 9JT, United Kingdom

Edited by Bruce L. Goode, Brandeis University, Waltham, MA, and accepted by Editorial Board Member Yale E. Goldman January 4, 2019 (received for review December 21, 2018)

The contractile actin cortex is a thin layer of filamentous actin, myosin motors, and regulatory proteins beneath the plasma membrane crucial to cytokinesis, morphogenesis, and cell migration. However, the factors regulating actin assembly in this compartment are not well understood. Using the *Dictyostelium* model system, we show that the three Diaphanous-related formins (DRFs) ForA, ForE, and ForH are regulated by the RhoA-like GTPase RacE and synergize in the assembly of filaments in the actin cortex. Single or double formin-null mutants displayed only moderate defects in cortex function whereas the concurrent elimination of all three formins or of RacE caused massive defects in cortical rigidity and architecture as assessed by aspiration assays and electron microscopy. Consistently, the triple formin and RacE mutants encompassed large peripheral patches devoid of cortical F-actin and exhibited severe defects in cytokinesis and multicellular development. Unexpectedly, many *forA*$^{-}$/*E*$^{-}$/*H*$^{-}$ and *racE*$^{-}$ mutants protruded efficiently, formed multiple exaggerated fronts, and migrated with morphologies reminiscent of rapidly moving fish keratocytes. In 2D-confinement, however, these mutants failed to properly polarize and recruit myosin II to the cell rear essential for migration. Cells arrested in these conditions displayed dramatically amplified flow of cortical actin filaments, as revealed by total internal reflection fluorescence (TIRF) imaging and iterative particle image velocimetry (PIV). Consistently, individual and combined, CRISPR/Cas9-mediated disruption of genes encoding mDia1 and -3 formins in B16-F1 mouse melanoma cells revealed enhanced frequency of cells displaying multiple fronts, again accompanied by defects in cell polarization and migration. These results suggest evolutionarily conserved functions for formin-mediated actin assembly in actin cortex mechanics.

actin cortex | formin | RhoGTPase | cell migration | cytokinesis

The actin-rich cell cortex is required for cell shape remodeling in fundamental cellular processes such as cytokinesis, morphogenesis, and cell migration (1). Cell motility is regulated by polarization, adhesion, and cytoskeletal activities leading to site-specific force generation, as exemplified by leading edge actin assembly and myosin-dependent rear contraction (2–4). Based on considerable variations of these activities in different cell types, this process is further subdivided into mesenchymal and amoeboid types of migration as two extremes of a wide spectrum (5). The slow mesenchymal type of motility is characterized by strong substrate adhesion and formation of prominent stress fibers as well as a protruding lamellipodium at the front (6), whereas fast amoeboid migration as exemplified by *Dictyostelium* cells is defined by weaker and more transient adhesions, a rounder cell shape, actin-rich protrusions or blebs in the front and myosin-driven contraction in the rear (7, 8). However, migration and other processes involving cell shape remodeling as, e.g., cytokinesis also require a thin, actin-rich cortex below the membrane.

This cortex contains actin, myosin, and associated factors assembling into a multicomponent layer (9, 10), which is intimately linked to the membrane in a phosphatidylinositol 4,5-bisphosphate [PI(4,5)P2]-dependent manner by the ezrin, radixin, and moesin (ERM) family of proteins in animal cells (11, 12) and cortexillin (Ctx) in *Dictyostelium* (13–15). The function of this thin actin meshwork is comparable to cell walls in plants, yeast, and bacteria, as it defines the cell's stiffness, resists external forces, and counteracts intracellular, hydrostatic pressure (9, 16). However, as opposed to the static cell wall of plants and bacteria, the actin cortex of amoebae and animal cells has viscoelastic properties that can be remodeled in the timescale of seconds. Rapid F-actin rearrangements enable cells to promptly modify their shapes for fast adaptation to changes in extracellular environment (9, 16). Moreover, and as opposed to cells with rigid cell walls encaging them entirely, cell cortex constituents of motile eukaryotic cells are organized in gradients due to the asymmetry of positioning signals (17).

The physical properties of the cell cortex such as its tension and contractility likely impacting on plasma membrane dynamics

Significance

The actin-rich cell cortex is a viscoelastic structure participating in a variety of cellular processes. However, the complete inventory of actin assembly factors driving its formation and knowledge about their specific contributions is still incomplete. We show here that functional integrity of the cell cortex in *Dictyostelium* and mammalian cells is backed up by multiple Diaphanous-related formins (DRFs) that are regulated by Rho-subfamily GTPases. These DRFs contribute to the generation of long actin filaments of the contractile actin cortex and are required for cell mechanics. Of note, these factors are excluded from Arp2/3 complex-nucleated networks, implying diversification of the cortex into functional subcompartments to segregate cortical actomyosin contraction in the rear or cleavage furrow ingression from actin-based protrusion in the front.

Author contributions: C.L., M.P., K.R., R.M., and J.F. designed research; C.L., S.B., A.C., T.S., V.D., J.D.-G., A.J., S.K., M.W., B.N., K.R., and J.F. performed research; C.L., B.N., and N.R. contributed new reagents/analytic tools; C.L., S.B., A.C., T.S., V.D., J.D.-G., A.J., S.K., M.W., M.P., K.R., R.M., and J.F. analyzed data; and S.B., M.P., K.R., and J.F. wrote the paper.

The authors declare no conflict of interest.

This article is a PNAS Direct Submission. B.L.G. is a guest editor invited by the Editorial Board.

[1]C.L. and S.B. contributed equally to this work.

[2]Deceased January 17, 2013.

[3]To whom correspondence should be addressed. Email: faix.Jan@mh-hannover.de.

This article contains supporting information online at www.pnas.org/lookup/suppl/doi:10.1073/pnas.1821638116/-/DCSupplemental.

Published online February 11, 2019.

are regulated by myosin motor activity as well as the arrangement and density of F-actin networks generated by distinct actin-assembly machineries (9). In cells, actin polymerization is mostly initiated by Arp2/3 complex and formins (18). The Arp2/3 complex creates branches at the sides of preexisting mother filaments and generates a dense actin meshwork at the front of migrating cells (18, 19). Formins instead nucleate and elongate long and linear actin filaments (19). A major subgroup of the formin family comprises Diaphanous-related formins (DRFs), which are autoinhibited due to intramolecular interactions of the Diaphanous inhibitory domain (DID) with the Diaphanous autoregulatory domain (DAD) (20). DRF autoinhibition is commonly released by binding of activated Rho-family GTPases (21, 22), but can also be driven by Ras (23). As yet, both Arp2/3 complex and formins have been implicated in the generation of cortical actin in different cell types (24, 25). However, the precise quantitative contributions of Arp2/3 complex- and formin-generated filaments to this structure and their interplay in cortical functions are still elusive. Depletion of the formin mDia1 (Diaph1) in HeLa cells led to failure of cortex function in mitotic cell division, while depletion of Arp2/3 complex alone did not (24). Interestingly, the same study reported Arp2/3 complex inhibition to potentiate effects of mDia1 depletion, suggesting synergistic activities of mDia1 and Arp2/3 complex in the nucleation of cortical actin (24). Atomic force microscopy (AFM) measurements indicated that cortical elasticity in HeLa and M2 melanoma cells is mostly affected by the formin inhibitor SmiFH2 (25). In contrast, reducing Arp2/3 complex activity by CK666 did not appear to play a critical role (25). These data suggested central roles for formins in cell cortex mechanics, but need to be complemented by genetics, last not least to identify specific, contributing formins.

Previously, we established that the mDia1-related formin ForA in *Dictyostelium* cells prevents blebbing in the rear to assist protrusion at the front, in particular under mechanical stress (18). Here, we identify and characterize two additional mDia-related, cortical *Dictyostelium* formins, ForE, and ForH, which synergize with ForA to safeguard cortex-dependent functions. Moreover, we extend our studies to mammalian formins mDia1 and -3, providing conclusive evidence that comparable pathways operate in higher eukaryotes.

Results

Active ForA Accumulates in the Cleavage Furrow of Dividing Cells. Consistent with the mechanistic similarities between migration and cytokinesis, many proteins accumulating in the trailing edge, as for instance myosin II, cortexillin (Ctx), the functional homolog of ERM proteins in *Dictyostelium*, and IQGAPs, were also found in cleavage furrows and are known to regulate cytokinesis (26–28). Thus, we explored the localization of active ForA at different stages of the cell cycle. Active ForA is uniformly localized in the cell cortex of unpolarized interphase cells (17). In mitotic cells, active ForA remained evenly distributed in the cell cortex up to early anaphase, but subsequently began to relocalize to the cleavage furrow like IQGAP1 and Ctx I (*SI Appendix*, Fig. S1 *A* and *B*), strongly suggesting a critical function of formin-generated cortical actin in cytokinesis, as previously shown in a variety of cell types (29). However, when cultivated in Petri dishes allowing adhesion of cells to the substratum, or even when exposed to high shear forces in shaken suspension culture, *forA*$^-$ cells exhibited negligible defects in cytokinesis (*SI Appendix*, Fig. S1 *C* and *D*). Of note, we have previously shown that either Ctx I and II or IQGAP1 and IQGAP2 had to be eliminated simultaneously to cause strong defects in cytokinesis, while single-knockout mutants exhibited no or minor defects (28). Thus, the lack of a cytokinesis defect in *forA*$^-$ cells suggested functional overlaps of ForA with one or multiple other cortical formins to safeguard this critical cellular function. In line with this view, cortical F-actin is still present in contractile regions of *forA*$^-$ cells, such as the trailing edge (17).

ForA Interacts with Active Form of the RhoA Homolog RacE. DRFs such as ForA are commonly assumed to be activated by GTP-bound Rho-family GTPases. *Dictyostelium* cells lack canonical Cdc42 and Rho homologs, but express 20 Rac proteins, some of which exert characteristics of Cdc42 and RhoA functions. Since appropriate ForA targeting and activation requires concurrent interactions with PI(4,5)P2 and an active GTPase (17), we employed yeast two-hybrid (Y2H) analyses to systematically screen all 20 *Dictyostelium* Racs for interaction with the N-terminal domain of ForA encompassing the GTPase-binding domain (GBD). Under the most stringent growth conditions on selective media, ForA genetically interacted with constitutively active RacA and RacE, while it failed to interact with dominant-negative variants of these GTPases (Fig. 1*A*). RacA has not yet been characterized, but contains a BTB domain at its C terminus and lacks a classical CAAX motif required for prenylation (30). Consistently, ectopically expressed RacA fused to GFP localized ubiquitously in the cytoplasm and was not enriched at the cell cortex (*SI Appendix*, Fig. S2). Thus, it appeared unlikely that it regulates recruitment and activation of ForA at the cortex. RacE instead was previously implicated in regulation of cortical tension and cleavage furrow progression (31). Since Y2H analyses can occasionally generate ambiguous results, we sought to corroborate these findings in an independent assay. To this end, we generated genetic knockout cell lines devoid of RacA and RacE in the AX2 WT strain (Fig. 1*B*). Then, we monitored localization of constitutively active ForA fused to GFP in these knockouts. As shown in Fig. 1*C*, ForA was normally targeted to the cell cortex in *racA*$^-$ cells, but failed to localize to the cortex in *racE*$^-$ cells, strongly suggesting a physiological interaction between ForA and RacE. Consistently, the purified N terminus of ForA also physically interacted with GMP-PNP–loaded RacE in pull-down experiments (Fig. 1*D*). In addition, constitutively active RacE was capable to release autoinhibition of an inactive formin sandwich complex formed by N- and C-terminal fragments of ForA in both pulldowns and pyrene assays (Fig. 1 *D* and *E*). Finally, we monitored localization of active RacE fused to YFP in cells in 2D-confinement, i.e., under a thin sheet of agar. Unlike previous work that failed to detect active RacE in the cleavage furrow of unconfined cells (32), the active GTPase accumulated about twofold in the cleavage furrow compared with pole regions upon 2D-confinement (Fig. 1*F*). Moreover, like active ForA, the GTPase was also markedly enriched in the rear cortex of migrating cells (Fig. 1*G* and Movie S1), substantiating the view that ForA is regulated by RacE.

Active RacE Additionally Interacts with Cortical Formins ForE and ForH. Based on the critical effect of RacE deficiency on cytokinesis, contractility and the regulation of ForA, and the fact that RacE constitutes the only known Rho-family GTPase in *Dictyostelium* with RhoA-like functions, we reasoned that additional formins may interact with the active GTPase and localize to the cell cortex to safeguard cortex functions. Thus, from the 10 formins expressed in *Dictyostelium* cells (33), we screened all 4 potential candidates expressed at the vegetative stage, referred to as ForB, ForE (dDia3), ForH (dDia2), and ForF (dDia1) with Rho- GTPases in the Y2H assay. ForI could be excluded from the screen because of lacking the regulatory GBD, and ForG was omitted due to its specific interaction with active Ras (23). Strong and specific interactions with active RacE were identified for two of the four tested formins. ForE interacted with active variants of RacE and RacF2 (Fig. 2*A*). However, since RacF2 appears to carry out specific functions in macrocyst formation during the sexual cycle (34), we did not follow that lead. Unexpectedly, active RacE also interacted with ForH (Fig. 2*B*), previously shown to operate in filopodia formation (35).

Next, we examined the subcellular localization of constitutively active ForE and ForH variants lacking the DAD regions and fused to YFP in freely moving or 2D-confined WT and

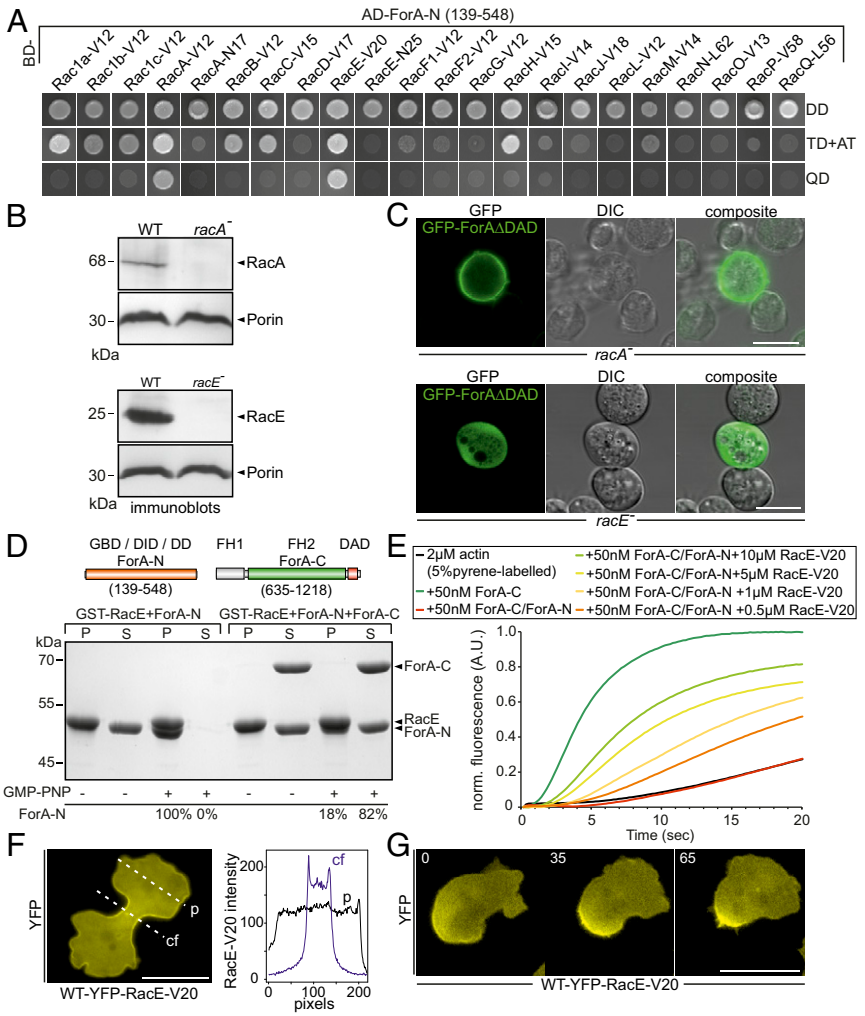

Fig. 1. ForA is regulated by the RhoA-homolog RacE. (*A*) The N-terminal domain of ForA (ForA-N) containing the GBD interacts specifically with the activated forms of RacA (RacA-V12) and RacE (RacE-V20) in the Y2H assay. Yeast was transformed with the indicated constructs and selected for the presence of prey and bait plasmids by growth on double-dropout (DD) media lacking leucine and tryptophan. Interactions were assayed by growth on stringent triple-dropout (TD) media additionally lacking histidine in the presence of 3 mM 3-amino-1,2,4-triazole (3-AT) and on quadruple-dropout (QD) media additionally lacking histidine and adenine. AD, Gal4-activation domain. (*B*) Genetic elimination of RacA and RacE was confirmed by immunoblotting. Porin was used as a loading control. (*C*) Constitutively active ForA fused to GFP requires RacE for targeting to the cell cortex but localizes appropriately in the absence of RacA. (Scale bars, 10 μm.) (*D*) ForA constructs used for biochemical analyses. Active RacE interacts directly with ForA-N and was able to partially release ForA-N from the autoinhibited ForA-N/ForA-C complex. GST-pulldown experiments with GMPPNP-loaded RacE are shown. The percentages below the lanes indicate the relative amounts of ForA-N in pellet (P) and supernatant (S) fractions. DD, dimerization domain; FH, formin homology domain. (*E*) Active RacE releases autoinhibition of the catalytically inactive ForA-N/ForA-C complex to promote actin assembly in pyrene assays in a concentration-dependent manner. (*F*) Active RacE N-terminally fused to YFP accumulates about twofold in the cell cortex of the cleavage furrow in 2D-confinement under agar. cf, cleavage furrow; p, pole. (Scale bar, 20 μm.) (*G*) Images from time-lapse movies correspond to Movie S1 and show that active RacE is enriched in the rear cell cortex of a polarized cell migrating under agar. (Scale bar, 20 μm.)

racE^{-} cells. Consistent with previous work (35), ectopic expression of active ForH in WT cells triggered the formation of numerous filopodia, with the active formin being markedly enriched at the cell cortex and filopodial tips (Fig. 2*C* and *SI Appendix*, Fig. S3). In 2D-confinement, filopodia formation was strongly suppressed and active ForH accumulated in the rear cortex of migrating cells, resembling localization of active ForA under the same conditions (17). To our surprise, and as opposed to the entirely diffuse localization of active ForA in *racE*$^{-}$ cells, constitutively active ForH was still able to trigger filopodia formation and accumulate in the cell cortex of freely moving *racE*$^{-}$ mutant cells. In 2D-confinement, however, the formin became largely cytosolic and failed to be incorporated into the rear.

Active ForE also markedly localized to the cortex of unconfined WT cells and to distal tips of filopodia (Fig. 2*D* and *SI Appendix*, Fig. S3). In the *racE*$^{-}$ mutant, however, the formin was not targeted to the cortex and remained diffuse in the cytoplasm under both experimental settings, implying a requirement for RacE signaling to mediate appropriate subcellular targeting. Consistently, and as previously shown for RacE (36), active ForA, ForE, and ForH localized in folate gradients after treatment with latrunculin B specifically on that portion of the plasma membrane facing lower chemoattractant concentrations (*SI Appendix*, Fig. S4). Thus, *Dictyostelium* cells express three RacE-regulated formins that accumulate in cell cortex and rear of cells migrating in 2D-confinement.

Elimination of the Three Cortical Formins Causes Drastic Cytokinesis and Developmental Defects. To uncover a potential functional redundancy of these three RacE-regulated, cortical formins, we eliminated them all either alone or in combination by gene disruption, to obtain a complete collection of single and double mutants as well as a cell line lacking all three formins (Fig. 3*A* and *SI Appendix*, Fig. S5). Mutant lines devoid of either ForA or ForH have previously been described (17, 35). Next, we asked whether, or to which extent, cytokinesis is impaired after consecutive elimination of these cortical formins. For that, we first assayed cytokinesis of the *forA*$^{-}$-single, the *forA*$^{-}$/*E*$^{-}$-double, and the *forA*$^{-}$/*E*$^{-}$/*H*$^{-}$-triple mutant at high stringency in shaken suspension, and compared effects obtained with RacE- and myosin II-null mutants known to exhibit strong defects in mitotic cell division under these conditions (37, 38). After fixing the cells together with DAPI, we quantified number of nuclei per cell as an unambiguous readout for cytokinesis defects. In cells harvested from shaken suspension after 48 h, the vast majority of WT cells and *forA*$^{-}$-single and *forA*$^{-}$/*E*$^{-}$-double mutants was mono- or binucleated, although a few *forA*$^{-}$/*E*$^{-}$-double mutant cells also displayed three or four nuclei (Fig. 3 *B* and *C*). By contrast, the *forA*$^{-}$/*E*$^{-}$/*H*$^{-}$-triple mutant exhibited a severe cytokinesis defect and was virtually indistinguishable from *racE*$^{-}$ and *mhcA*$^{-}$ mutants, since about 90% of these mutants developed highly multinucleated cells (Fig. 3 *B* and *C*). To exclude the possibility that a specific formin executes a predominant function in cytokinesis, we additionally performed these cytokinesis assays

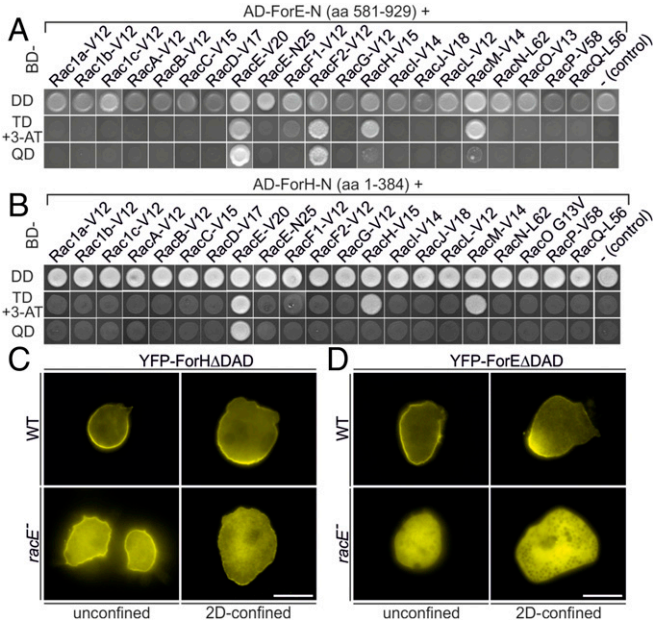

Fig. 2. Active RacE interacts with two additional cortical formins. (*A* and *B*) ForE-N and ForH-N interact specifically with the active form of RacE (V20) in the Y2H assay. Yeast was transformed with the indicated constructs and selected for the presence of prey and bait plasmids by growth on double-dropout (DD) media lacking leucine and tryptophan. ForE-N additionally showed strong interaction with active RacF2 (V12). Interactions were scored by growth on stringent triple-dropout (TD) media in the presence of 3 mM 3-amino-1,2,4-triazole (3-AT) or quadruple-dropout (QD) media as outlined in Fig. 2. Both formins showed no genetic interaction using the dominant-negative RacE (N25) variant or empty Gal4-activation domain (AD) plasmids as negative controls. BD, Gal4-binding domain. (*C* and *D*) Constitutively active ForF and ForE localize in the cell cortex and rear of migrating WT cells. YFP-tagged variants of the formins were expressed in WT and *racE*$^-$ cells and analyzed by wide-field fluorescence microscopy at the conditions indicated. (Scale bars, 10 μm.)

with all three combinations of double-mutant cells. Although mutant cells lines lacking ForH had a stronger tendency to form multinucleated cells, about 80% of all three formin double-null mutants still contained cells with only one or two nuclei (*SI Appendix*, Fig. S6). Thus, a severe cytokinesis defect was only manifested after inactivation of all three cortical formins.

Importantly, multicellular development also depends on contractility and cortical integrity. Myosin II mutants for instance cannot advance beyond the aggregation stage (39) and double mutants devoid of Ctx I/Ctx II known to tether cortical actin filaments to the membrane entirely fail to develop (40). Thus, we additionally compared multicellular development of WT cells and *forA*$^-$-single, *forA*$^-$/*E*$^-$-double, and the *forA*$^-$/*E*$^-$/*H*$^-$-triple mutant on bacterial lawns. Similar to WT, single and double formin mutants were still able to advance through development and produce viable spores, although fruiting bodies of the *forA*$^-$/*E*$^-$-double mutant already appeared considerably smaller (Fig. 4*D*). Notably, the *forA*$^-$/*E*$^-$/*H*$^-$-triple mutant was completely blocked in development and not even able to aggregate. Thus, consistent with their overlapping functions in cytokinesis, all three formins have to be eliminated simultaneously to abrogate morphogenesis.

ForA, ForE, and ForH Synergize in the Maintenance of Cortical Integrity. To quantify the assumed synergistic role of these formins in cortical integrity in the absence of adhesion forces, and to directly compare their contributions to this with those of RacE, we performed micropipette aspiration assays (MPAs) of resuspended WT and mutant cells to measure their global mechanical resistance. To avoid secondary responses of the highly dynamic *Dictyostelium* cells to external suction pressure, we quantified the initial projection length (Lp) of cells captured from suspension at a constant pressure of 500 Pa in MPAs. Serial elimination of the formins correlated with increasing defects of cortical rigidity and peaked in the *forA*$^-$/*E*$^-$/*H*$^-$-triple mutant with an average indentation length of 13 ± 6.7 μm (mean ± SD) as opposed to 3 ± 1.2 μm in WT cells (Fig. 4 *A* and *B*). In contrast to many WT cells, *forA*$^-$/*E*$^-$/*H*$^-$ cells were unable to withdraw from the micropipette even at this comparably low suction pressure, and all of them were ultimately sucked into the pipette within 5–10 min (Movie S2). *RacE*$^-$ cells also exhibited a major defect of cortical rigidity with an Lp of 11 ± 5.1 μm, although the defect was slightly weaker compared with the formin triple-knockout mutant. Unexpectedly, albeit none of the analyzed cells was able to completely withdraw from the pipette, almost all cells (98%) resisted complete aspiration at 500 Pa within 10 min. Finally, we also measured the cortical properties of mutant cells lacking the Arp2/3-complex activator Scar and the actin filament elongator VASP. Cortex rigidity of *scrA*$^-$ and *vasP*$^-$ cells was also clearly impaired compared with control. However, the contribution of Scar and of VASP was moderate, since measured Lp values were only in the range of the formin single-knockout mutants. Thus, in *Dictyostelium* Arp2/3 complex and VASP appear to contribute far less to mechanical rigidity of the cortex compared with formins.

Next, we examined the distribution of cortical F-actin in fixed WT, *forA*$^-$/*E*$^-$/*H*$^-$ and *racE*$^-$ cells after phalloidin staining. Additionally, we labeled the specimens for PI(4,5)P2-binding Ctx, to visualize the lipid gradient between front and rear in polarized *Dictyostelium* cells. In highly polarized WT cells, the bulk of F-actin was concentrated in the leading edge and contained only small amounts of Ctx, while the rear and lateral sides, encompassing the thin layer of cortical actin, were strongly enriched for Ctx (Fig. 4*C*). By contrast, *forA*$^-$/*E*$^-$/*H*$^-$ and *racE*$^-$ mutants were rounder overall and did not show the characteristic Ctx differential. Most notably, large sections of the cortex in both mutants were devoid of the cortical actin layer, while remaining segments of the cortex still contained prominent F-actin assemblies. Quantification of phalloidin fluorescence intensities across

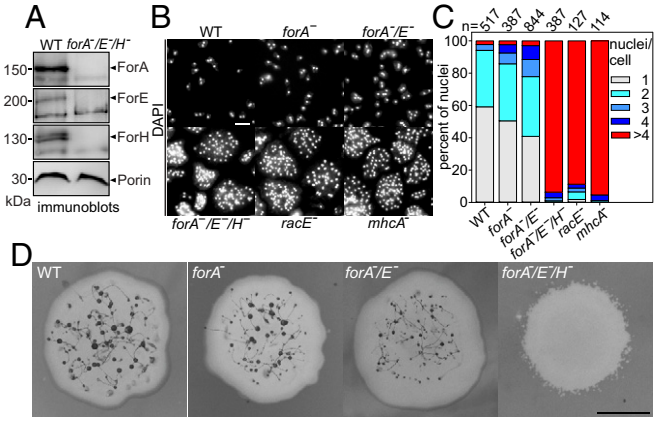

Fig. 3. Elimination of all three cortical formins is detrimental for cell division and development. (*A*) Inactivation of the *forA*, *forE*, and *forH* genes in the triple-KO mutant was verified by immunoblotting using specific formin sera. Porin was used as a loading control. (*B*) WT and the mutant cells indicated were grown for 48 h in shaken suspension at 150 rpm, subsequently seeded on glass coverslips, fixed, and stained with DAPI to visualize the nuclei. (Scale bar, 20 μm.) (*C*) Quantification of nuclei in cells as shown in *B*. n, number of analyzed cells. (*D*) Coincident elimination of ForA, ForE, and ForH blocks development. WT or formin-deficient cells were transferred with a tooth pick onto a lawn of *Klebsiella aerogenes* on nonnutrient agar plates and monitored after 96–120 h of development. (Scale bar, 0.5 mm.)

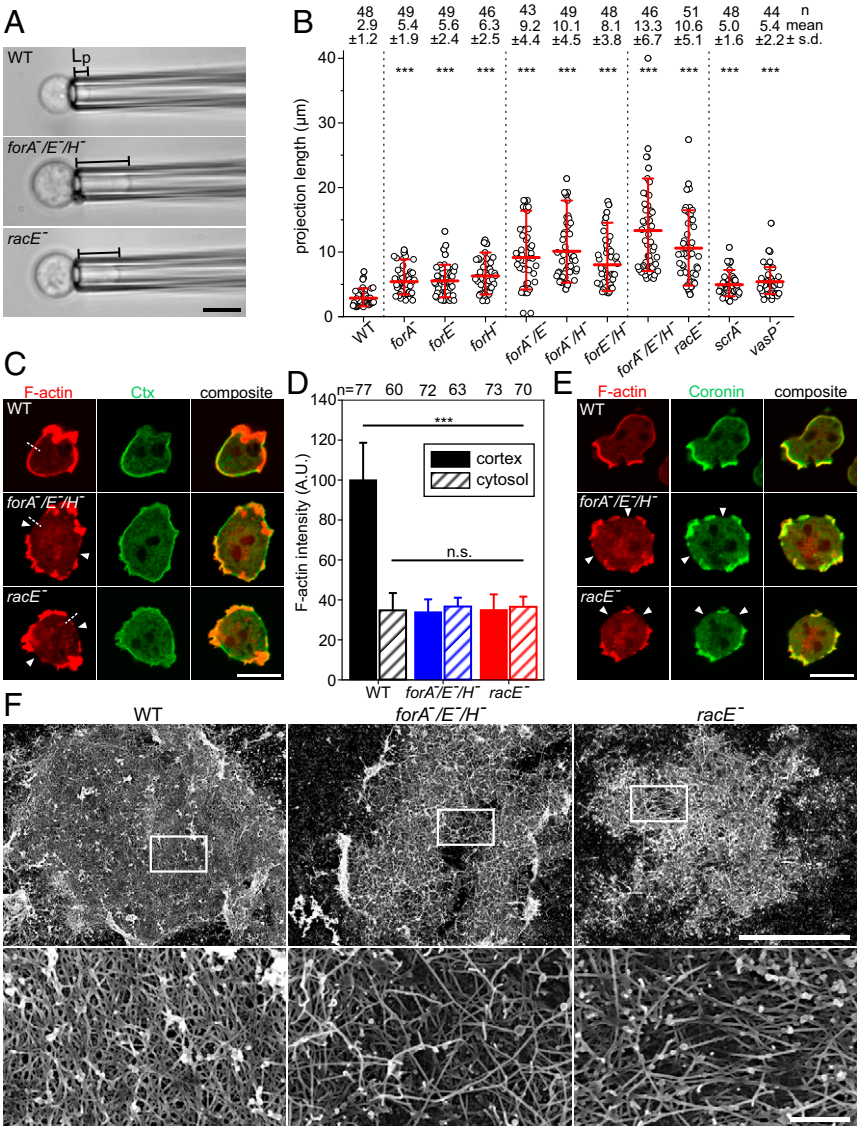

Fig. 4. Elimination of the three cortical formins or of RacE increasingly impairs cortical rigidity and disrupts the contractile actin cortex. (*A*) Lp of WT and the mutant cells indicated was determined by micropipette aspiration using a constant suction pressure of 500 Pa from time-lapse movies; data correspond to Movie S2. (Scale bar, 10 μm.) (*B*) Quantitative analysis of the projection lengths of probed cells. ***$P < 0.001$ by Mann–Whitney rank sum test. n, number of analyzed cells. Statistical differences refer to WT. (*C*) Defects of the actin cortex in *forA*$^-$/*E*$^-$/*H*$^-$ and *racE*$^-$ mutants. Fixed WT and mutant cells were stained with a monoclonal Ctx antibody (green) to visualize PI(4,5)P2-containing membranes and F-actin with phalloidin (red). The white arrow heads indicate regions of low cortical density in the mutants. (Scale bar, 10 μm.) (*D*) Quantification of cortical and intracellular actin in WT and mutant cells. Average intensity profiles along five-pixel-wide lines as shown in *C* by the white dashed lines. n, number of analyzed cells; error bars, SDs. (*E*) Prominent F-actin assemblies outside the cortical breaches in *forA*$^-$/*E*$^-$/*H*$^-$ and *racE*$^-$ cells are identified as protrusions containing coronin (green), particularly marking Arp2/3 complex-driven actin networks, and phalloidin-stained F-actin (red). (Scale bar, 10 μm.) (*F*) Representative SEM micrographs of detergent-extracted WT and mutant cells (low magnification overviews on *Top* and high magnification of *Insets* at *Bottom*, respectively). [Scale bars: overview, 5 μm; *Insets*, 0.5 μm.]

the cortex in actin-deficient areas confirmed this view (Fig. 4*D*), and was further substantiated by time-lapse imaging of WT and mutant cells expressing the F-actin probe LimEΔcoil-GFP (Movie S3). We hypothesized that the thin layer that is missing in the mutants corresponds to the contractile actin cortex, whereas the remaining and prominent F-actin assemblies represent Arp2/3 complex-driven F-actin structures such as leading edges or endocytic cups. Thus, we labeled WT and mutant cells with phalloidin and for the F-actin binding protein coronin, which is a central constituent of Arp2/3 complex-mediated F-actin networks (41). Consistent with the key function of Arp2/3 complex in protrusion, coronin was strongly enriched in the leading edges of WT cells (Fig. 4*E*). Notably, coronin was depleted from actin-deficient regions, but colocalizing with the prominent F-actin assemblies in *forA*$^-$/*E*$^-$/*H*$^-$ and *racE*$^-$ mutants, strongly suggesting that these structures are nucleated by Arp2/3 complex. Finally, we explored the ultrastructural cortex architecture by scanning EM (SEM) after detergent extraction of cells. As opposed to the dense, cortical meshwork of WT cells with numerous overlapping filaments, elimination of the three formins or of RacE caused marked differences in cortical actin organization, including a lower filament density interspaced with large gaps containing much fewer filaments with different geometry (Fig. 4*F*).

Cortical Formins Are Essential for Motility in 2D-Confinement. Loss of ForA was previously shown to affect cell migration in unconfined and 2D-confined scenarios (17). Thus, we analyzed random cell migration of freely moving and 2D-confined *forA*$^-$/*E*$^-$/*H*$^-$ and *racE*$^-$ mutants in phosphate buffer employing phase-contrast time-lapse microscopy, and compared migration rates of the mutants to that of WT cells. Additionally, we also determined mean square displacement (MSD) to discriminate locally restricted movement or wiggling of cells from effective directional cell migration (42). Intriguingly, elimination of ForA, ForE, and ForH or of RacE even increased the speed of randomly migrating, mutant cells in unconfined environments to 8.2 ± 2.1 μm·min^{-1} (*forA*$^-$/*E*$^-$/*H*$^-$) or 8.9 ± 2.1 μm·min^{-1} (*racE*$^-$) (mean ± SD) compared with WT controls with 6.8 ± 1.8 μm·min^{-1} (Fig. 5 *A* and *B*). However, when compressed under a sheet of agar, *forA*$^-$/*E*$^-$/*H*$^-$ and *racE*$^-$ mutants were abrogated for migration (1.9 ± 0.59 μm·min^{-1} and 1.8 ± 0.4 μm·min^{-1}), as assessed by tracking of the centroids compared with WT (4.8 ± 1.9 μm·min^{-1}) (Fig. 5 *C* and *D*). Consistent with their higher motility in unconfined settings, a large proportion of both mutants were more directional and had higher MSD values compared with control (Fig. 5*E*). In marked contrast, the MSD values of both mutants virtually dropped to zero in 2D-confinement, illustrating

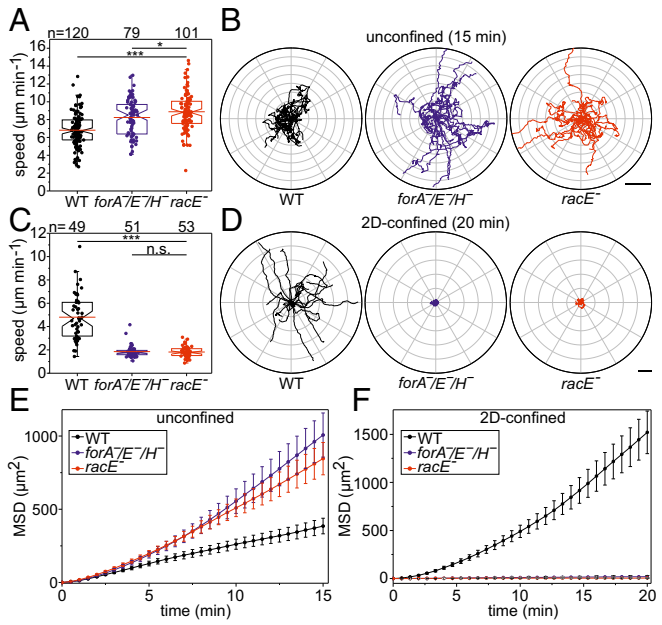

Fig. 5. *ForA⁻/E⁻/H⁻* and *racE⁻* mutants cannot migrate in 2D-confinement. (*A* and *C*) Box plots summarizing the random migration speed of WT, *ForA⁻/E⁻/H⁻* and *racE⁻* cells in unconfined (*A*) and 2D-confined (*C*) conditions. At least three movies from three independent experiments were analyzed for each cell type. n.s., not significant; $*P < 0.05$; $***P < 0.001$ by Mann–Whitney rank sum test. n, number of cells analyzed. (*B* and *D*) Radar plots showing the trajectories of 20 randomly migrating WT, *ForA⁻/E⁻/H⁻*, and *racE⁻* cells in unconfined and 2D-confined conditions as indicated. Note the high directional persistence of the mutant cells in unconfined settings. (Scale bars: *B*, 30 μm; *D*, 20 μm.) (*E* and *F*) Analysis of the mean square displacement of WT, *ForA⁻/E⁻/H⁻*, and *racE⁻* cells migrating in unconfined and 2D-confined conditions as indicated. Error bars represent standard error of the mean; n as in *A* and *C*.

their inability to migrate under agar, whereas WT cells were still able to efficiently migrate under these conditions (Fig. 5*F*). These findings substantiate the fundamental role of the contractile actin cortex for cell migration in confinement.

Mutants Lacking Cortical Formins or RacE Form Multiple Fronts. Amoeboid cells such as *Dictyostelium* cells generally exhibit only weak adhesion to the substrate to allow for fast migration in unconfined settings. In *Dictyostelium* cells impaired in the cortical actin cytoskeleton, cell behavior or establishment and maintenance of cell shape are expected to be more severely affected by changes in membrane tension. To test this hypothesis, we imaged freely moving *forA⁻/E⁻/H⁻* and *racE⁻* mutants at high magnification by time-lapse phase contrast microscopy, and compared their activities to those of WT cells. WT cells were more spherical and typically formed one or two protruding fronts in the form of pseudopods or macropinosomes at a given time. By contrast, *forA⁻/E⁻/H⁻* and *racE⁻* mutants were considerably flatter, as evidenced by strongly reduced halos in phase-contrast images at their cell boundaries. Notably, about 33% of *forA⁻/E⁻/H⁻* cells and 19% of *racE⁻* cells intermittently exhibited a fan-shaped, keratocyte-like morphology and migrated with high, directional persistence, which was contrasted by only 6% of highly directional WT cells (Movie S4). Remarkably, both mutants often developed multiple fronts exhibiting five or six lamellipodia-like pseudopods (Fig. 6 *A* and *B* and Movie S5). The elimination of formins and of RacE also substantially increased the combined protrusion area relative to total cell area in the mutants by more than 30% to 32.0% ± 5.7% (*forA⁻/E⁻/H⁻*) and 29.2% ± 2.0% (*racE⁻*) compared with WT control (19.6% ± 1.7%, Fig. 6*C*). Moreover, the protrusion speed of the fronts in the mutants was about doubled to 0.19 ± 0.03 μm·s^{-1} (*forA⁻/E⁻/H⁻*) and 0.20 ± 0.03 μm·s^{-1} (*racE⁻*) compared with WT control (0.10 ± 0.02 μm·s^{-1}) (Fig. 6*D*). Interestingly, inhibition of myosin II by blebbistatin had little effect on the motility of *ForA⁻/E⁻/H⁻* and *racE⁻* mutant cells (*SI Appendix*, Fig. S7), excluding augmented actomyosin contractility as direct cause for these effects. Although reflection interference contrast microscopy (RICM) analyses revealed a larger contact area of mutant cells (*SI Appendix*, Fig. S8 *A* and *B*), they formed fewer actin foci, and these adhesion points were significantly shorter lived than those in controls (*SI Appendix*, Fig. S8 *C–E*). In line with these observations, the contact area of multiple front- or keratocyte-shaped cells was inhomogeneous and interspersed with less adhesive sections, as evidenced by RICM (Movies S6 and S7). Thus, the combination of increased protrusive activity and decreased adhesiveness in the mutants may explain the high directional persistence in motility assays. Finally, we noticed that the growth of initially formed fronts in the mutants typically ceased when multiple, competing protrusions were formed on the opposite side of the cell. In these cases, initial fronts rapidly lost adhesion to the underlying surface and were effectively retracted into the cell body (*SI Appendix*, Fig. S9 and Movies S6 and S8).

Polarity Defects and Dramatically Increased Cortical Actin Flow in *forA⁻/E⁻/H⁻* and *racE⁻* Mutants. An intact contractile actin cortex of amoeboid cells regulates cell migration in 2D-confinement by guiding hydrostatic pressure, created by actomyosin contraction in the rear, to the front to promote leading edge protrusion (17). Thus, we monitored myosin II and F-actin representing the two main components of the contractile machinery in WT and mutant cells after mechanical stress in confinement under agar.

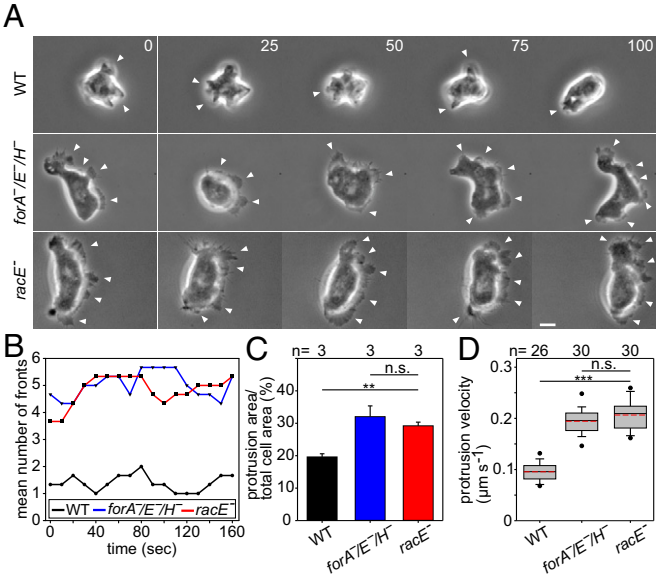

Fig. 6. *ForA⁻/E⁻/H⁻* and *racE⁻* mutants form multiple and faster protruding fronts. (*A*) Gallery with stills from a phase-contrast time-lapse series of randomly migrating WT and mutant cells in unconfined settings corresponding to Movie S5 shows the recurring formation of multiple fronts (white arrow heads) in *ForA⁻/E⁻/H⁻* and *racE⁻* mutants. Time is in seconds. (Scale bar, 5 μm.) (*B*) Quantification of the average number of protruding fronts in migrating WT and mutant cells as shown in *A*. (*C*) Quantification of the ratio of protrusion area over total cell area in WT and indicated mutant cells. Error bars represent standard error of the mean. n.s., not significant; $**P < 0.01$ by Mann–Whitney rank sum test. (*D*) Average protrusion velocities of fronts in WT and mutant cells. Boxes include 50% and whiskers 80% of all measurements, and dots represent the 5th/95th percentile. n.s., not significant; $***P < 0.001$ by Mann–Whitney rank sum test. n, number of cells analyzed.

WT cells expressing fluorescently tagged heavy chain of myosin II were highly polarized, and the motor protein was continuously concentrated in a compact, crescent-like sheet at the rear cortex beneath the plasma membrane (Fig. 7*A* and Movie S9). In striking contrast, *forA*$^{-}$/*E*$^{-}$/*H*$^{-}$ and *racE*$^{-}$ mutants remained highly unpolarized in 2D-confinement, as evidenced by the aberrant circular localization of myosin II in a band-like fashion along most of the cell periphery, albeit this phenotype was slightly less prominent in *racE*$^{-}$ cells (Fig. 7*A*). Moreover, myosin II did not accumulate in a crisp band as in WT cells, but was dispersed into multiple, string-like assemblies in the mutants. Myosin II was also largely dislodged from the membrane and was instead strongly enriched at an endoplasm-ectoplasm interface separating the organelle free area from the cell interior (Fig. 7*A*). Consistently, time-lapse imaging of the mutant cells revealed a highly erratic behavior of myosin II associated with intense blebbing, substantiating the massive defects in the contractile cell cortex of mutant cells (Movie S9). Quantification of myosin II bandwidth as well as its radial distribution in WT and mutant cells in polarity plots corroborated this view (Fig. 7*B*).

We then analyzed the dynamic behavior of cortical actin filaments at the ventral plasma membrane by total internal reflection fluorescence (TIRF) microscopy in WT and mutant cells after confinement under agar. In WT cells, cortical actin, visualized by the F-actin marker LimEΔcoil-GFP, was organized into a delicate, filamentous web, interspaced with dynamic actin foci, which accumulated most strongly in protruding fronts evidently driven by Arp2/3 complex-mediated actin assembly (Fig. 7*C* and Movie S10). A filamentous network was also observed in the *forA*$^{-}$/*E*$^{-}$/*H*$^{-}$ and *racE*$^{-}$ mutants. However, presumably due to the high membrane tension and their strong polarization defect in 2D-confinement, they did not form protruding fronts. Moreover, as assessed from TIRF time-lapse imaging, the dynamics of cortical actin filaments was drastically changed compared with control. These filaments were rapidly pulled into the cell center in a process reminiscent of actin retrograde flow in higher eukaryotes. Particle image velocimetry (PIV)-based quantification of cortical actin flow confirmed this notion (Fig. 7*D*). The velocity distribution showed flows of up to 72 μm·min^{-1} in *racE*$^{-}$ cells and almost up to 100 μm·min^{-1} in the *forA*$^{-}$/*E*$^{-}$/*H*$^{-}$ mutant compared with the average flow of 1.48 ± 1.08 μm·min^{-1} (mean ± SD) in WT cells (Fig. 7*E*). Consistently, PIV analyses further revealed that the regions with fastest actin filament flows overlap with myosin II-enriched regions in *forA*$^{-}$/*E*$^{-}$/*H*$^{-}$ and *racE*$^{-}$ mutants (Fig. 7 *A* and *E* and *SI Appendix*, Fig. S10). Together, these data strongly suggest that filaments nucleated by cortical formins regulate subcellular myosin II localization and cortical actin flow under mechanical stress.

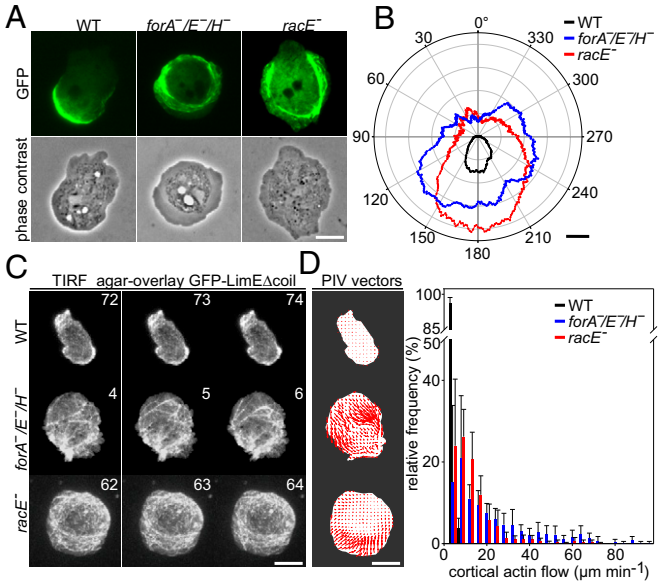

Fig. 7. *ForA*$^{-}$/*E*$^{-}$/*H*$^{-}$ and *racE*$^{-}$ mutants cannot polarize and exhibit a drastically increased cortical flow in 2D-confinement. (*A*) The characteristic localization of GFP-myosin II in the rear cortex of WT cells is abolished in *forA*$^{-}$/*E*$^{-}$/*H*$^{-}$ and *racE*$^{-}$ mutant cells illustrating a major defect in polarization. Still images from time-lapse movies correspond to Movie S9. (Scale bar, 10 μm.) (*B*) Quantification of the width of the cortical myosin layer in WT and mutant cells determined by rotational analysis of the fluorescence signal from cells as shown in *A*. Radar plot shows the mean myosin II band thickness of the cell lines indicated. (Scale bar, 0.5 μm.) (*C*) Still images from TIRF time-lapse movies of WT and mutant cells expressing the F-actin probe GFP-LimEΔcoil in 2D-confined conditions under agar. Time is in seconds. (Scale bar, 10 μm.) (*D*) PIV analyses of cortical actin flow in WT and mutant cells. Five consecutive frames recorded at 0.5-s intervals corresponding to Movie S10 were used for PIV analysis. The resulting vectors mark the mean actin velocity per frame (*Left*). Distribution of actin flow velocities of the cell lines reveal a strikingly increased actin flow in the mutants (*Right*). Error bars are standard error of the mean.

Cell Lines Lacking Murine mDia1 and -3 Display Phenotypes Indicative of Conserved, Cortical Functions. To explore whether our observations are generalizable to higher eukaryotes, we analyzed mammalian formins in highly motile B16-F1 mouse melanoma cells. Since mDia subfamily formins (1–3) are regulated by RhoA (43), which is well established to drive contractility, we focused on subcellular localization of EGFP-tagged mDia variants after ectopic expression in B16-F1 cells. Consistent with our previous findings (17), we found constitutively active mDia1 variants, i.e., mDia1ΔDAD as well as the newly designed point mutant mDia1-FL-2xAla (M1182A and F1195A), which is expected to release autoinhibition of the FL protein (21), to localize prominently in the cell rear, whereas the full-length, autoinhibited protein remained cytosolic (Fig. 8*A*). Virtually identical results were obtained with corresponding mDia3 variants (Fig. 8*A*), whereas active mDia2 was not found in the cell rear, but mostly targeted to filopodia tips (44). To evaluate mDia functions in the mammalian cell cortex, we employed CRISPR/Cas9-mediated disruption of the genes encoding mDia1 and -3, both individually and in combination in B16-F1 cells. Loss of respective protein in independent, clonal cell lines was confirmed by immunoblotting (Fig. 8*B*). Interestingly, mDia1 levels were evidently increased in both mDia3-KO cell lines, and vice versa, indicative of compensatory, regulatory mechanisms presumably serving to sustain sufficient levels of these cortical formins (Fig. 8*B*). Phalloidin stainings revealed defects in cell polarization as well as markedly increased frequencies in mDia1 and -3 single mutants of cells forming multiple fronts, a phenotype that was even further increased in mDia1/3 double-KO cells (Fig. 8 *C* and *D*) and strikingly reminiscent of cortical formin pathway KOs in *Dictyostelium*. Next, we analyzed random cell migration of B16-F1 WT and mutant cells on laminin using time-lapse, phase-contrast microscopy. Interestingly, as opposed to *Dictyostelium* cells migrating without 2D-confinement, cell depolarization, and apparent stimulation of the multiple front phenotype reduced the efficiency of the highly adhesive mode of melanoma cell migration, likely caused by inefficient protrusion in a productive, migratory direction. Specifically, whereas single mDia1 and -3 mutants displayed a moderate but statistically significant reduction of migration rate in this assay (by 11.7%), removal of both mDia1 and -3 decreased migration even further (by 18.4%; Fig. 8*E*). Together, these data strongly suggest the RhoA effectors of the mDia formin subfamily, in particular, mDia1 and -3, to exert functions in the actin cortex that are conserved in evolution from *Dictyostelium* to mammals.

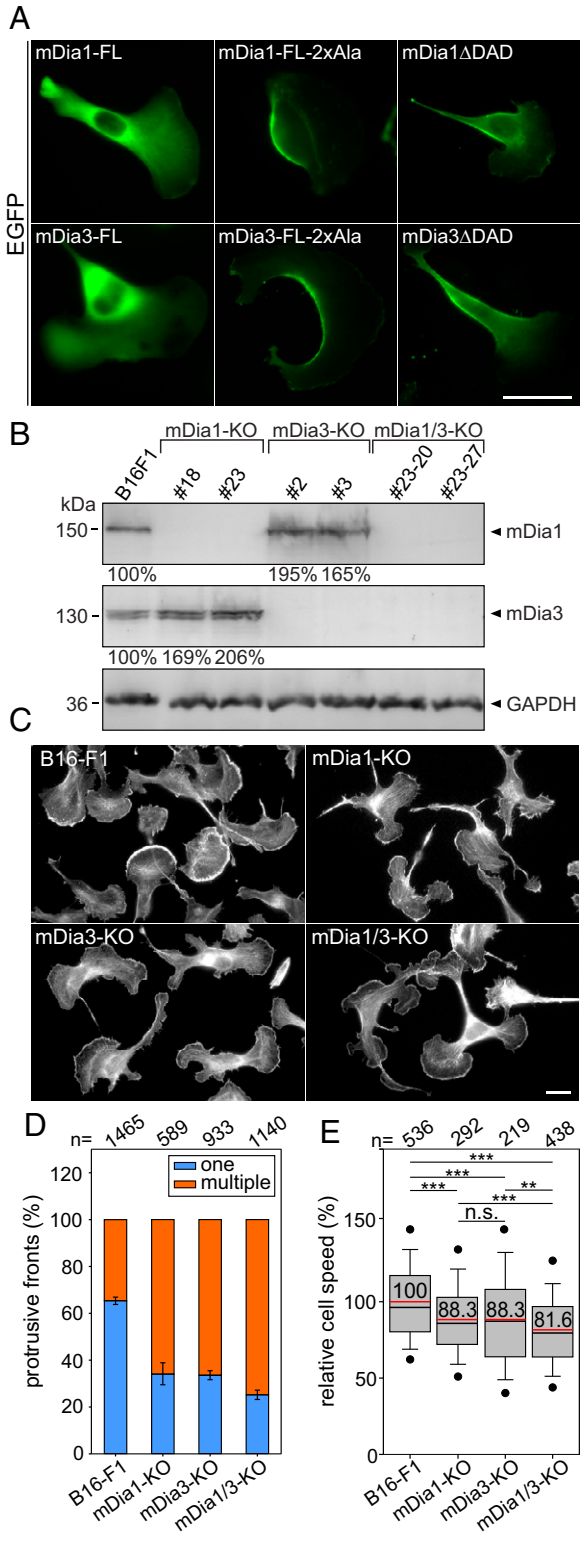

Fig. 8. Formation of multiple fronts and defects in polarization and migration in mDia1- and/or -3-deficient B16-F1 cells. (*A*) Subcellular localization of EGFP-mDia1 and -3 variants in B16-F1 cells migrating on laminin. While full-length (FL) mDia1 and -3 were cytosolic and largely excluded from protrusive fronts, constitutively active mDia1-FL-2xAla (M1182A and F1195A), mDia1ΔDAD, mDia3-FL-2xAla (M1057A and F1170A), and mDia3ΔDAD strongly accumulated in the rear cortex. (Scale bar, 20 μm.) (*B*) Immunoblotting of individual and combined mDia1 and mDia3 KO clones as indicated. GAPDH: loading control. Numbers below respective lanes indicate relative changes of mDia1 and -3 expression levels normalized to GAPDH. (*C*) Polarization defects and formation of multiple fronts in respective cell types, as revealed by phalloidin staining. Note increasingly pronounced multiple-front phenotypes in single versus double (mDia1/3) KO cells. (Scale bar, 10 μm.) (*D*) Quantification of protrusive fronts (one versus multiple) from images as shown in *C*. Error bars, standard error of the mean from at least six independent experiments, n, cell number. (*E*) Quantification of random migration of respective cell types on laminin. Boxes include 50% and whiskers 80% of all measurements; dots represent the fifth/95th percentile. n.s., not significant; $^{**}P < 0.01$; $^{***}P < 0.001$ by Mann–Whitney rank sum test. n, number of tracked cells.

Discussion

Over 30 years ago, Bray and White postulated that cortical contractility may not only contribute to retraction of the trailing edge, but also to ingression of the cleavage furrow during cytokinesis (45). Since then, localization and participation in both processes has been demonstrated for numerous cell cortex components including myosin II (46), Ctx (27), PTEN (47), and IQGAP family members (28). Here, we demonstrated that three DRFs, ForA, ForE, and ForH, act synergistically in the assembly of actin filaments in the contractile actin cortex as evidenced by the increasing severity of additive KO phenotypes, which directly correlated with a gradual decrease in mechanical cortex rigidity. We also showed that the active form of the Rho family GTPase, RacE, binds to the GBD of ForA, releasing its autoinhibition to initiate actin assembly. RacE shows considerable sequence similarity with Rho proteins from other species and represents the closest homolog of mammalian RhoA in *Dictyostelium* (36, 48). The phenotype of *racE*$^-$ cells was similar to that of the triple KO DRF cells, including large cytokinesis defects in suspension (31) as well as large effects on development (36). This reinforces the idea that the DRFs are required for actin filament formation, and this is regulated by RacE. Moreover, RacE localizes to the cell rear as well as cleavage furrow in mitotic cells, and is essential for cortical localization of ForA and ForE.

Similar to the redundancy in cortical actin organization exhibited by DRFs in *Dictyostelium*, we also found stronger, complementary phenotypes after combined inactivation of the formins mDia1 and -3 in B16-F1 mouse melanoma cells. This redundancy of the microfilament system is a common phenomenon for essential cellular activities, and has been observed previously for the actin cross-linking proteins α-actinin and filamin (49) and for Ctx I and II (50) in *Dictyostelium*. While ForA, ForE, and ForH act synergistically in actin filament assembly in the contractile actin cortex, it is likely that they also have isoform-specific roles and can be activated by other signaling pathways. For example, we found that constitutively active ForH localized to the cortex in unconfined *racE*$^-$ cells, but remained largely cytosolic after compression in 2D-confinement, suggesting multiple interactors mediate its subcellular targeting. Of these, RacE is presumably important for ForH targeting under mechanical stress. Incidentally, ForH was recently also found as potential RacE interactor by mass spectrometry (51). In addition, active ForH and ForE also trigger filopodia formation, but as both cortex and filopodia constitute F-actin structures directly associated with the plasma membrane, these actin assembly factors may well participate in the formation of various membrane-associated structures entailing long, unbranched filaments.

The strong effects on cytokinesis and cortex-dependent functions in *forA*$^-$/*E*$^-$/*H*$^-$ are similar to those found in *racE*$^-$ cells. This indicates the phenotypic effect of *racE* gene elimination to derive from the lack of forA/E/H activation. Consistent with this, none of WT formins (ForA, ForE or ForH) localized to the cortex in these cells as they are likely autoinhibited (*SI Appendix*, Fig. S11 and ref. 17). We also found that active RacE accumulates in the cleavage furrow of mitotic cells upon 2D-confinement, implying that it plays a role in regulating cytokinesis by recruitment and activation of cortical formins at this site.

CELL BIOLOGY

Both *forA*$^{-}$/*E*$^{-}$/*H*$^{-}$ and *racE*$^{-}$ mutants displayed flat morphologies and formation of multiple, dynamic multidirectional protrusions along the cell contour. In agreement with recent work analyzing enhanced expansion of lamellipodial networks upon reduction of plasma membrane load (2), and considering theoretical calculations of cortex mechanics (52), these data imply that cells harboring a compromised viscoelastic cell cortex may experience reduced resistance to actin polymerization forces in protrusions. If correct, this could well cause the formation of amplified protrusions and multiple fronts observed in our mutants. Multiple protrusion formation in *Dictyostelium* was accompanied by adhesion weakening and irregular detachment. Consequently, most unconfined *forA*$^{-}$/*E*$^{-}$/*H*$^{-}$ and *racE*$^{-}$ cells, in some instances resembling fan-shaped keratocytes, migrated faster and more directionally than their WT controls. These phenotypes appeared at the expense of the more amoeboid type of migration usually seen in *Dictyostelium*.

Of note, the inhibition of myosin II by blebbistatin had little effect on the motility of keratocytes (53) as well as *ForA*$^{-}$/*E*$^{-}$/*H*$^{-}$ and *racE*$^{-}$ mutant cells (*SI Appendix*, Fig. S7). This indicates that the migratory modes adopted by these cell types and/or experimental conditions are less dependent on cortical contractility than during amoeboid or canonical, mesenchymal migration, and additionally mostly driven by the amplified network expansion activity at the leading edges of these cells (54). Interestingly, the migratory behavior of *Dictyostelium* cells can be switched from amoeboid to keratocyte-like by either decreasing PI(4,5)P2 levels or increasing Ras/Rap signaling (55). Whether or not these phenotypes could relate to the molecular mechanisms described here will be an exciting topic of future study.

In 2D-confinement, *forA*$^{-}$/*E*$^{-}$/*H*$^{-}$ and *racE*$^{-}$ mutants are unable to localize myosin II properly to the cell cortex, polarize, and migrate. Symmetry breaking obtained by an anisotropic distribution of components including myosin II drives both rear retraction in directed cell migration and cytokinesis. How myosin II is localized to the cell cortex is still not fully understood, but has been proposed to include signaling and mechanical cues including myosin phosphorylation by MHCK-A, PTEN, Ctx I, or talin in *Dictyostelium* (14, 47, 56, 57) or preferential binding to stretched actin filaments (59). In any case, a severely perturbed cortical actin cytoskeleton will likely interfere with myosin II positioning and activity in all these pathways. Our findings thus establish cortical formins as key to the establishment of polarity and properly regulated migration in both *Dictyostelium* and mammalian cells.

Consistent with the elimination of these formins or their activator RacE, SEM and live-cell TIRF imaging revealed cortical filament density in *forA*$^{-}$/*E*$^{-}$/*H*$^{-}$ and *racE*$^{-}$ cells to be reduced compared with WT, but raised the question as to which assembly factors are involved in generating the remaining cortical actin filaments. Our immunofluorescence results with fixed cells indicated these filaments to be primarily nucleated by remaining prominent actin assembly factors, such as Arp2/3 complex and VASP, although we cannot exclude at this stage the presence of filaments assembled by other formins, for instance, ForG, known to cooperate with Arp2/3 complex in large scale endocytosis (23) or by ForF (dDia1), which homogenously accumulates in the entire pseudopod (59).

In 2D-confinement, *forA*$^{-}$/*E*$^{-}$/*H*$^{-}$ and *racE*$^{-}$ mutants exhibited exceptionally fast centripetal flows of residual cortical filaments at velocities of 50–100 μm/min, which were contrasted by almost immobile cortical networks relative to the advancement of migrating, WT cells. This suggests that in 2D-confinement, *Dictyostelium* does not primarily use retrograde actin fluxes to drive force transmission during migration, as recently proposed for other cell types utilizing amoeboid motility (60, 61). However, the precise cause of the excessive cortical actin flows observed in the mutants remains to be clarified. An intact cortical cytoskeleton harbors various transmembrane proteins and receptors, potentially acting as barriers constraining lateral diffusion (62). Thus, we speculate that the increased cortical flows observed in our mutants are caused by diminished viscosities of their perturbed cortical networks.

Our initial characterization of genome-edited B16-F1 mouse melanoma mutants devoid of mDia1, mDia3, or both formins revealed striking similarities to the *Dictyostelium* system. Comparable to *Dictyostelium* ForA, ForE, and ForH, both mammalian formins are regulated by Rho-subfamily proteins, which are ultimately linked to contractility. Active variants of mDia1 and -3 but not the autoinhibited full-length proteins localized prominently to the rear cortex in polarized B16-F1 cells, and the individual elimination of these formins triggered the formation of multiple protrusive fronts as well as substantial defects in polarization and migration. The fact that the phenotypes were noticeably amplified in double mutants reinforced the conclusion of their overlapping functions. This is consistent with a very recent study analyzing the contractile actin cortex in Sertoli cells of mouse seminiferous tubules (63). Loss of mDia1 and -3 in these cells compromised the cortical actin cytoskeleton, leading to less dense F-actin meshworks ultimately resulting in impaired spermatogenesis. Taken together, our results suggest that formins are important in cell cortex establishment and maintenance, and that these functions are evolutionarily conserved across far distant organisms.

Materials and Methods

A complete description of the methods is provided in *SI Appendix, SI Materials and Methods*. This description includes construct generation, cell culture, transfections, and establishment of *Dictyostelium* and B16-F1 mutants, protein purification, actin assembly and pull-down assays, antibodies and immunoblots, imaging, aspiration assays, analyses of cell migration, Y2H assays, quantification of actin flows, and statistical analyses.

ACKNOWLEDGMENTS. We thank Annette Breskott for technical assistance and all members of the group for inspiring discussions. We further thank Martin Fuller for help with critical-point drying and Stuart Micklethwaite and John Harrington (Leeds Electron Microscopy and Spectroscopy Centre) for help with collecting SEM images. This work was supported by the Elite Network Bavaria (N.R.), Welcome Trust Grant 094231/Z/10/Z (to M.P.), intramural funding from the Helmholtz Society (to R.M. and K.R.), and Deutsche Forschungsgemeinschaft Grants GRK2223/1 (to K.R.) and FA 330/12-1 (to J.F.).

1. Blanchoin L, Boujemaa-Paterski R, Sykes C, Plastino J (2014) Actin dynamics, architecture, and mechanics in cell motility. *Physiol Rev* 94:235–263.
2. Mueller J, et al. (2017) Load adaptation of lamellipodial actin networks. *Cell* 171:188–200.e16.
3. Kage F, et al. (2017) FMNL formins boost lamellipodial force generation. *Nat Commun* 8:14832.
4. Sackmann E (2015) How actin/myosin crosstalks guide the adhesion, locomotion and polarization of cells. *Biochim Biophys Acta* 1853:3132–3142.
5. Paluch EK, Aspalter IM, Sixt M (2016) Focal adhesion-independent cell migration. *Annu Rev Cell Dev Biol* 32:469–490.
6. Bear JE, Haugh JM (2014) Directed migration of mesenchymal cells: Where signaling and the cytoskeleton meet. *Curr Opin Cell Biol* 30:74–82.
7. Charras GT, Coughlin M, Mitchison TJ, Mahadevan L (2008) Life and times of a cellular bleb. *Biophys J* 94:1836–1853.
8. Yoshida K, Soldati T (2006) Dissection of amoeboid movement into two mechanically distinct modes. *J Cell Sci* 119:3833–3844.
9. Clark AG, Wartlick O, Salbreux G, Paluch EK (2014) Stresses at the cell surface during animal cell morphogenesis. *Curr Biol* 24:R484–R494.
10. Chugh P, et al. (2017) Actin cortex architecture regulates cell surface tension. *Nat Cell Biol* 19:689–697.
11. Fehon RG, McClatchey AI, Bretscher A (2010) Organizing the cell cortex: The role of ERM proteins. *Nat Rev Mol Cell Biol* 11:276–287.
12. Maniti O, et al. (2012) Binding of moesin and ezrin to membranes containing phosphatidylinositol (4,5) bisphosphate: A comparative study of the affinity constants and conformational changes. *Biochim Biophys Acta* 1818:2839–2849.
13. Stock A, et al. (1999) Domain analysis of cortexillin I: Actin-bundling, PIP(2)-binding and the rescue of cytokinesis. *EMBO J* 18:5274–5284.
14. Ren Y, et al. (2009) Mechanosensing through cooperative interactions between myosin II and the actin crosslinker cortexillin I. *Curr Biol* 19:1421–1428.
15. Kee Y-S, et al. (2012) A mechanosensory system governs myosin II accumulation in dividing cells. *Mol Biol Cell* 23:1510–1523.

16. Salbreux G, Charras G, Paluch E (2012) Actin cortex mechanics and cellular morphogenesis. *Trends Cell Biol* 22:536–545.
17. Ramalingam N, et al. (2015) A resilient formin-derived cortical actin meshwork in the rear drives actomyosin-based motility in 2D confinement. *Nat Commun* 6:8496.
18. Rottner K, Faix J, Bogdan S, Linder S, Kerkhoff E (2017) Actin assembly mechanisms at a glance. *J Cell Sci* 130:3427–3435.
19. Pollard TD (2007) Regulation of actin filament assembly by Arp2/3 complex and formins. *Annu Rev Biophys Biomol Struct* 36:451–477.
20. Kühn S, Geyer M (2014) Formins as effector proteins of Rho GTPases. *Small GTPases* 5: e29513.
21. Lammers M, Rose R, Scrima A, Wittinghofer A (2005) The regulation of mDia1 by autoinhibition and its release by Rho*GTP. *EMBO J* 24:4176–4187.
22. Li F, Higgs HN (2005) Dissecting requirements for auto-inhibition of actin nucleation by the formin, mDia1. *J Biol Chem* 280:6986–6992.
23. Junemann A, et al. (2016) A *Diaphanous*-related formin links Ras signaling directly to actin assembly in macropinocytosis and phagocytosis. *Proc Natl Acad Sci USA* 113: E7464–E7473.
24. Bovellan M, et al. (2014) Cellular control of cortical actin nucleation. *Curr Biol* 24: 1628–1635.
25. Fritzsche M, Erlenkämper C, Moeendarbary E, Charras G, Kruse K (2016) Actin kinetics shapes cortical network structure and mechanics. *Sci Adv* 2:e1501337.
26. Fukui Y, Inoué S (1991) Cell division in *Dictyostelium* with special emphasis on actomyosin organization in cytokinesis. *Cell Motil Cytoskeleton* 18:41–54.
27. Weber I, et al. (1999) Cytokinesis mediated through the recruitment of cortexillins into the cleavage furrow. *EMBO J* 18:586–594.
28. Faix J, et al. (2001) Recruitment of cortexillin into the cleavage furrow is controlled by Rac1 and IQGAP-related proteins. *EMBO J* 20:3705–3715.
29. Bohnert KA, Willet AH, Kovar DR, Gould KL (2013) Formin-based control of the actin cytoskeleton during cytokinesis. *Biochem Soc Trans* 41:1750–1754.
30. Rivero F, Dislich H, Glöckner G, Noegel AA (2001) The Dictyostelium discoideum family of Rho-related proteins. *Nucleic Acids Res* 29:1068–1079.
31. Gerald N, Dai J, Ting-Beall HP, De Lozanne A (1998) A role for Dictyostelium racE in cortical tension and cleavage furrow progression. *J Cell Biol* 141:483–492.
32. Larochelle DA, Vithalani KK, De Lozanne A (1997) Role of Dictyostelium racE in cytokinesis: Mutational analysis and localization studies by use of green fluorescent protein. *Mol Biol Cell* 8:935–944.
33. Rivero F, et al. (2005) A comparative sequence analysis reveals a common GBD/FH3-FH1-FH2-DAD architecture in formins from Dictyostelium, fungi and metazoa. *BMC Genomics* 6:28.
34. Muramoto T, Urushihara H (2006) Small GTPase RacF2 affects sexual cell fusion and asexual development in Dictyostelium discoideum through the regulation of cell adhesion. *Dev Growth Differ* 48:199–208.
35. Schirenbeck A, Bretschneider T, Arasada R, Schleicher M, Faix J (2005) The diaphanous-related formin dDia2 is required for the formation and maintenance of filopodia. *Nat Cell Biol* 7:619–625.
36. Wang Y, Senoo H, Sesaki H, Iijima M (2013) Rho GTPases orient directional sensing in chemotaxis. *Proc Natl Acad Sci USA* 110:E4723–E4732.
37. Chen P, Ostrow BD, Tafuri SR, Chisholm RL (1994) Targeted disruption of the Dictyostelium RMLC gene produces cells defective in cytokinesis and development. *J Cell Biol* 127:1933–1944.
38. Larochelle DA, Vithalani KK, De Lozanne A (1996) A novel member of the rho family of small GTP-binding proteins is specifically required for cytokinesis. *J Cell Biol* 133: 1321–1329.
39. Springer ML, Patterson B, Spudich JA (1994) Stage-specific requirement for myosin II during Dictyostelium development. *Development* 120:2651–2660.
40. Shu S, Liu X, Kriebel PW, Daniels MP, Korn ED (2012) Actin cross-linking proteins cortexillin I and II are required for cAMP signaling during *Dictyostelium* chemotaxis and development. *Mol Biol Cell* 23:390–400.
41. Bretschneider T, et al. (2002) Dynamic organization of the actin system in the motile cells of Dictyostelium. *J Muscle Res Cell Motil* 23:639–649.
42. Litschko C, et al. (2017) Differential functions of WAVE regulatory complex subunits in the regulation of actin-driven processes. *Eur J Cell Biol* 96:715–727.
43. Lammers M, Meyer S, Kühlmann D, Wittinghofer A (2008) Specificity of interactions between mDia isoforms and Rho proteins. *J Biol Chem* 283:35236–35246.
44. Block J, et al. (2008) Filopodia formation induced by active mDia2/Drf3. *J Microsc* 231: 506–517.
45. Bray D, White JG (1988) Cortical flow in animal cells. *Science* 239:883–888.
46. Moores SL, Sabry JH, Spudich JA (1996) Myosin dynamics in live Dictyostelium cells. *Proc Natl Acad Sci USA* 93:443–446.
47. Pramanik MK, Iijima M, Iwadate Y, Yumura S (2009) PTEN is a mechanosensing signal transducer for myosin II localization in Dictyostelium cells. *Genes Cells* 14:821–834.
48. Vlahou G, Rivero F (2006) Rho GTPase signaling in Dictyostelium discoideum: Insights from the genome. *Eur J Cell Biol* 85:947–959.
49. Witke W, Schleicher M, Noegel AA (1992) Redundancy in the microfilament system: Abnormal development of Dictyostelium cells lacking two F-actin cross-linking proteins. *Cell* 68:53–62.
50. Faix J, et al. (1996) Cortexillins, major determinants of cell shape and size, are actin-bundling proteins with a parallel coiled-coil tail. *Cell* 86:631–642.
51. Senoo H, Cai H, Wang Y, Sesaki H, Iijima M (2016) The novel RacE-binding protein GflB sharpens Ras activity at the leading edge of migrating cells. *Mol Biol Cell* 27: 1596–1605.
52. Sens P, Plastino J (2015) Membrane tension and cytoskeleton organization in cell motility. *J Phys Condens Matter* 27:273103.
53. Keren K, Yam PT, Kinkhabwala A, Mogilner A, Theriot JA (2009) Intracellular fluid flow in rapidly moving cells. *Nat Cell Biol* 11:1219–1224.
54. Keren K (2011) Cell motility: The integrating role of the plasma membrane. *Eur Biophys J* 40:1013–1027.
55. Miao Y, et al. (2017) Altering the threshold of an excitable signal transduction network changes cell migratory modes. *Nat Cell Biol* 19:329–340.
56. Steimle PA, et al. (2001) Recruitment of a myosin heavy chain kinase to actin-rich protrusions in Dictyostelium. *Curr Biol* 11:708–713.
57. Tsujioka M, et al. (2012) Talin couples the actomyosin cortex to the plasma membrane during rear retraction and cytokinesis. *Proc Natl Acad Sci USA* 109:12992–12997.
58. Uyeda TQP, Iwadate Y, Umeki N, Nagasaki A, Yumura S (2011) Stretching actin filaments within cells enhances their affinity for the myosin II motor domain. *PLoS One* 6: e26200.
59. Winterhoff M, et al. (2014) The diaphanous-related formin dDia1 is required for highly directional phototaxis and formation of properly sized fruiting bodies in Dictyostelium. *Eur J Cell Biol* 93:212–224.
60. Bergert M, et al. (2015) Force transmission during adhesion-independent migration. *Nat Cell Biol* 17:524–529.
61. Liu Y-J, et al. (2015) Confinement and low adhesion induce fast amoeboid migration of slow mesenchymal cells. *Cell* 160:659–672.
62. Ostrowski PP, Grinstein S, Freeman SA (2016) Diffusion barriers, mechanical forces, and the biophysics of phagocytosis. *Dev Cell* 38:135–146.
63. Sakamoto S, et al. (2018) mDia1/3 generate cortical F-actin meshwork in Sertoli cells that is continuous with contractile F-actin bundles and indispensable for spermatogenesis and male fertility. *PLoS Biol* 16:e2004874.